

## RESEARCH ARTICLE

# A Flyback Converter With Novel Active Dissipative Snubber

YEU-TORNG YAU<sup>1,2</sup>, (Member, IEEE), AND TSUNG-LIANG HUNG<sup>3</sup><sup>1</sup>Department of Ph.D. Program, Prospective Technology of Electrical Engineering and Computer Science, National Chin-Yi University of Technology, Taichung 41170, Taiwan<sup>2</sup>Department of Electrical Engineering, National Chin-Yi University of Technology, Taichung 41170, Taiwan<sup>3</sup>Asian Power Device Inc., Taoyuan 33058, Taiwan

Corresponding author: Yeu-Torng Yau (pabloyau@ncut.edu.tw)

This work was funded by Asian Power Device Inc.

**ABSTRACT** The active clamp flyback converters (ACF) can provide features of high power density and high power efficiency. However, ACF is usually applied to in the applications of medium-to-high power range. For a low power application, the ACF may not be a cost-efficient choice. The flyback converter with a lossless snubber can provide high efficiency for low-power application, but it needs an additional inductor and generates more electromagnetic interference (EMI) emissions. The circuit designers also consider the balance between conversion efficiency, size, and cost. Based on the reasons above, the flyback converter with dissipative RCD snubber is still popular in the applications of low-to-medium power range. When the dissipative snubber is adopted to reduce EMI in the power converters, it increases the loss and hence reduces the efficiency. In this paper, a new concept, called active dissipative snubber, is proposed to suppress the resonance in the discontinuous conduction mode (DCM). In the proposed active dissipative snubber, the digital controller activates the dissipative snubber only when the EMI noise is occurring, then disabled after the noise is decayed or disappears. Digital logic makes the passive snubber smart, which can selectively absorb the EMI noise. Since the proposed snubber is not connected to the main circuit all the time, it can provide lower power loss, but still performs better EMI emissions and maintains conversion efficiency.

**INDEX TERMS** Dissipative snubber, lossless snubber, flyback converter, EMI.

## I. INTRODUCTION

First, the definition list of symbols and variables in this paper is shown in Table 1. Fig. 1 shows a typical flyback converter with synchronous rectifier (SR) control. The SR IC [1] can detect  $v_{d2}$  and  $v_{s2}$  of  $Q_2$  to generate an accurate driving signal  $v_{g2}$  to  $Q_2$ .

To improve the conversion efficiency at light load, the commercial control ICs [2], [3] of flyback converters will not only enter the discontinuous conduction mode (DCM), but also reduce the switching frequency [2], [3], [4], [5], [6] or operate in the valley-skipping mode (VSM) [2], [3], [4], [5], [6] to reduce PWM frequency and switching loss further.

When  $L_m$  is totally demagnetized to make  $i_{Lm}$  zero, and then  $C_{oss1}$  of  $Q_1$  resonates with  $L_m$  and  $L_{LK}$  [7], [8] with

The associate editor coordinating the review of this manuscript and approving it for publication was Tariq Masood<sup>1</sup>.

ringing  $v_{ds1}$  and  $v_{N2}$  as shown in Fig. 2.  $v_{N1}$ ,  $v_{ds1}$ ,  $v_{s2}$ , and  $v_{N2}$  have multi-period resonance in DCM or VSM. However, the parasitic resistance of the circuit trace and components dissipates the resonance energy.

The switching period is long enough to ensure that the energy of the resonant tank is totally exhausted before the next switching period starts, even without any external snubber.

However, the ringing  $v_{N2}$  and  $v_{ds1}$  increase the electromagnetic interference (EMI) noise emissions within the frequency range from about 200 kHz to 1 MHz [9]. These ringing voltages induce common-mode EMI emissions [10], [11]. That means that the resonance needs to be suppressed as fast as possible.

The conventional dissipative RC snubbers [8], [12], [13], [14] and RCD snubbers [8], [12], [13], [14] make the resonant voltage amplitude decay by an exponential envelope

TABLE 1. Nomenclature.

Symbols and veria	Description
$V_{in}, V_o$	Input voltage and output voltage, respectively
$GND_1, GND_2$	Ground nets of primary side and secondary side, respectively
$Q_1$	Main power switch
$C_{oss1}$	Output capacitance of $Q_1$
$Q_2$	Synchronous rectifier
$T_1$	Main transformer
$L_m$	Magnetizing inductance
$L_{LK}$	Leakage inductance
$T_r$	Resonant period of $L_m$ and $C_{oss1}$
$f_r$	Resonant frequency of $L_m$ and $C_{oss1}$
$N_1, N_2$	Primary and secondary windings of $T_1$ , respectively
$n_{sp}$	Turn ratio of $N_2$ over $N_1$
$C_o$	Output capacitor
$Q_3$	Switch of snubber
$R_s$	Resistor of current sensor
$R_{sn}$	Resistor of snubber
$C_{sn}$	Capacitor of snubber
$D_{clamp}$	Clamping diode of snubber
$V_{N1}, V_{N2}$	Voltage of windings $N_1$ and $N_2$ , respectively
$i_{N1}, i_{N2}$	Current of windings $N_1$ and $N_2$ , respectively
$v_{gs1}$	Voltage of gate to source of $Q_1$
$v_{ds1}, v_{ds2}$	Voltage of drain to source of $Q_1$ and $Q_2$ , respectively
$v_{s2}, v_{g2}, v_{d2}$	Voltage of source, gate, drain of $Q_2$ , respectively
$v_{g3}$	Gate voltage of $Q_3$
$T_{on}, T_{off}$	Conduction time and disconnection time of $Q_1$ , respectively

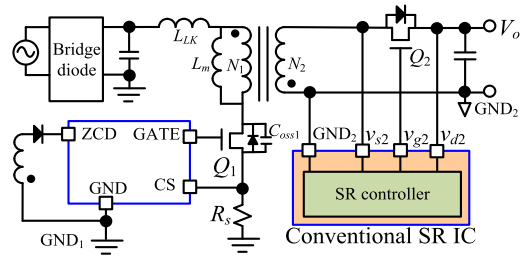


FIGURE 1. Typical flyback converter with synchronous rectifier.

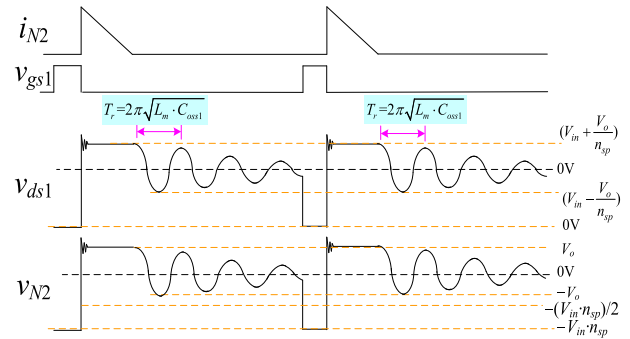


FIGURE 2. Waveforms of a flyback converter with conventional dissipative snubber in DCM and VSM.

line, so the resonance voltage is still high in the first few resonance periods as shown in Fig. 2. The EMI emissions from resonance voltage and current can be detected by the EMI receiver.

The active clamp flyback converter (ACF) [15], [16], [17] is a well-known solution, which can provide features of high power density and high power efficiency. However, the ACF is usually applied to medium-to-high power applications due to its system complex, which needs a high voltage half bridge driver and 3 active switches. For a low power application, the ACF may not be a cost-efficient design. The flyback converter with a lossless snubber [11], [18], [19], [20], [21], [22], [23], [24] can provide high efficiency but it needs an additional magnetic component and generates significant EMI emissions [11]. Additionally, the resonance of  $L_m$  and  $C_{oss1}$  still exists in VSM mode.

Based on the reasons above, flyback converters with dissipative clamp snubbers are still suitable solutions for low-to-medium applications. The dissipative snubbers can be located at the primary-side winding [8], [12], [13], [14] or the secondary-side winding [12] of the main transformer. The typical two types of dissipative snubbers of the secondary side are shown in Fig. 3. The drawback of a conventional dissipative snubber is its fixed connection to the main circuit to make continuous operation, thereby leading to power dissipation.

In this paper, a new active dissipative snubber with digital controller is proposed, which activates the dissipative snubber only when the noise is occurring, then disabled after the noise source is decayed or disappears. The digital controller drives the dissipator to selectively decay EMI noise. The

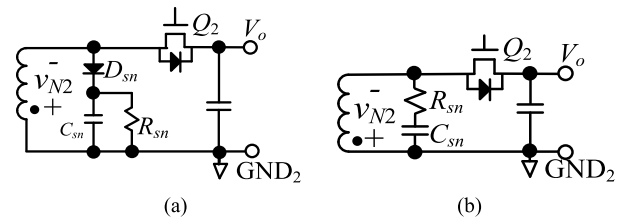


FIGURE 3. Two dissipative secondary-side snubber circuits: (a) RCD snubber; (b) RC snubber.

proposed method can provide better EMI performance than the traditional dissipative snubber, but still maintains similar conversion efficiency.

## II. PROPOSED CIRCUIT CONFIGURATION

As shown in Fig 4, the conventional dissipative snubber is connected to the main circuit for a long time  $T_{off}$  in each switching period. Long time connection to main circuit results in unnecessary power consumption besides the resonant energy of  $L_m$  and  $C_{oss1}$ .

As shown in Fig. 5, the concept of the proposed snubber can detect the first valley of resonance period on  $v_{N2}$  and absorb the resonance energy in half the resonance period with a strong dissipator. After the resonant energy of  $L_m$  and  $C_{oss1}$  is exhausted, the proposed snubber is disconnected from the  $v_{N2}$  to avoid more unnecessary power loss.

The commercial SR control IC can detect the accurate time of  $T_{off}$  and  $i_{N2}$ . The proposed snubber detects  $v_{N2}$  and  $v_{g2}$  of the SR IC. When  $Q_1$  is turned off, the digital block in the proposed snubber starts to count the number of the resonant

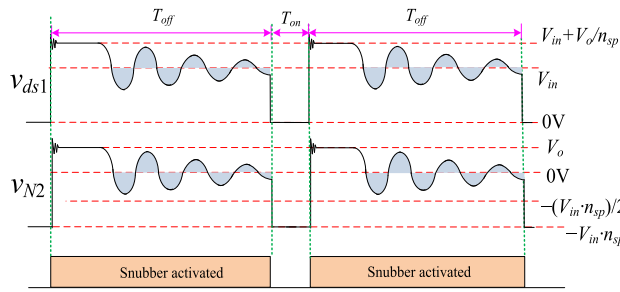


FIGURE 4. Waveforms of  $v_{ds1}$  and  $v_{N2}$  of SR flyback with the conventional dissipative snubber.

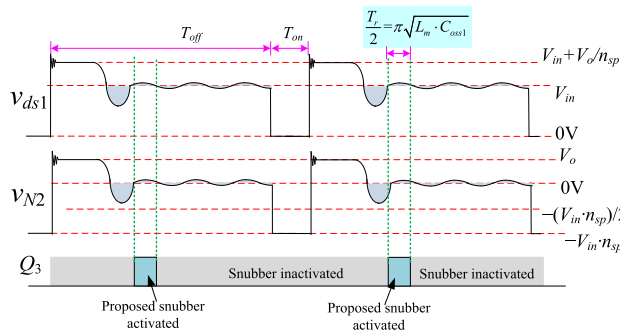


FIGURE 5. Waveforms of  $v_{ds1}$  and  $v_{N2}$  of SR flyback converter with the proposed snubber.

valley of  $v_{N2}$ , and turns on  $Q_3$  to enable the dissipator on the first positive resonance wave. Therefore, the dissipator is connected to the winding  $N_2$  to clamp  $v_{N2}$ .

Since, the strong dissipator is connected to  $v_{N2}$ , so that the stored energy of the resonance tank of  $L_m$  and  $C_{oss1}$  can be quickly dissipated in half the resonant period. However, the dissipator can result in significant energy loss, so it is necessary to disable the dissipator after the first resonant cycle until the next switching period. The proposed snubber can reduce the signal intensity of the quasi peak (QP) and the average of the conducted EMI emissions.

According to the concept above, Fig. 6 also shows the implemented circuit structure for the proposed snubber, which can detect  $v_{g2}$  from the SR control IC and  $v_{s2}$  to determine the operation timing. The snubber includes a digital logic controller, an energy dissipater, and an active switch  $Q_3$ . The digital logic controller is realized with the complex programmable logic device (CPLD) chip.

The energy dissipater can be realized with a well-known RC snubber or RCD snubber, which usually consists of a diode  $D_{clamp}$ , a resistor  $R_{sn}$ , and a capacitor  $C_{sn}$  as shown in Fig. 6.

By considering the average efficiency, the commercial flyback converters usually adopt a multi-operation mode with CCM, critical conduction mode (CRM), DCM, and VSM as shown in Fig. 7. Therefore, the proposed snubber controller is designed to support the multi-operation mode. The digital controller senses  $v_{g2}$  and  $v_{s2}$  to determine its operation mode in each switching period. In CCM and CRM, the resonance

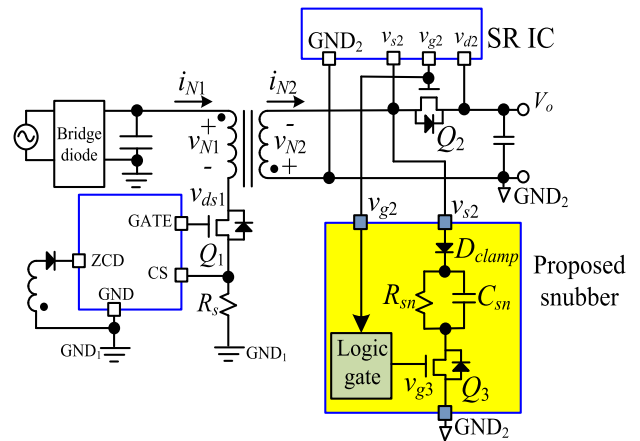


FIGURE 6. SR flyback converter with the proposed active dissipative snubber.

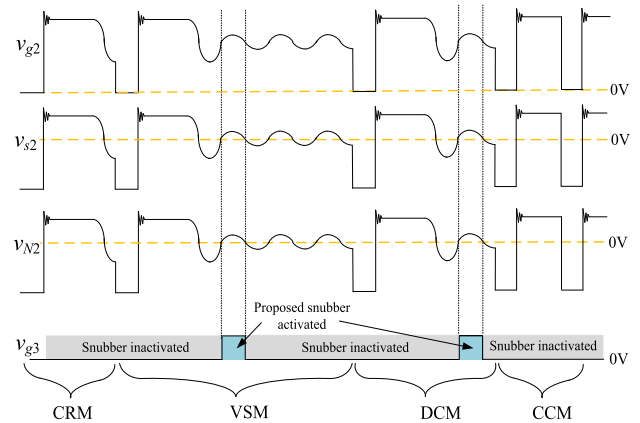


FIGURE 7. Operation modes of the SR flyback converter with the proposed snubber.

of  $L_m$  and  $C_{oss1}$  and the first positive resonance wave do not happen as shown in Fig. 7. Therefore, the digital controller disables the dissipator. This means that the dissipator will not be activated in CCM and CRM. In DCM or VSM, the dissipator only connects to the main circuit for a short time. So, the proposed snubber has lower energy loss than the traditional dissipative snubber with full-time connection to the main circuit. That is to say, the power loss of the proposed snubber in CCM and CRM is theoretically the same equivalent model as in Fig. 1. The detailed process of the snubber controller is represented as a finite state machine in Fig. 8. Fig. 8(a) shows the simplified controller circuit. There are 3 comparators to detect the signals of  $v_{g2}$  and  $v_{s2}$  to result in 6 logic states, which is called Actions 1 to 6.

Comparator 1 compares  $v_{g2}$  and  $\frac{-V_{in}}{2} \left( \frac{N_2}{N_1} \right) > v_{N2}$  to obtain Actions 1 and 2. The comparator 2 compares  $v_{s2}$  and GND level to obtain Actions 3 and 4. The comparator 3 compares  $v_{g2}$  and  $(v_{s2} + v_{th2})$  to obtain Actions 5 and 6.

When  $\frac{-V_{in}}{2} \left( \frac{N_2}{N_1} \right) > v_{N2}$ , the output of comparator 1 is logic “true” for Action 1, and else is logic “false” for Action 2. When  $v_{s2} > 0$ , the output of comparator 2 is logic

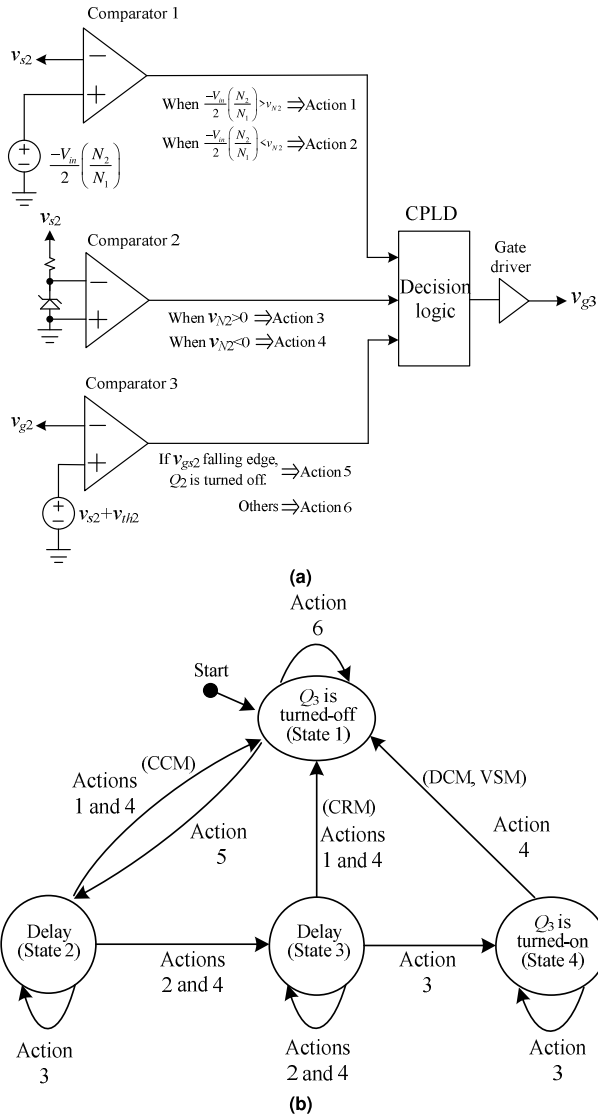


FIGURE 8. Finite state machine of the proposed snubber.

“true” for Action 3, and else is logic “false” for Action 4. When the falling edge of  $v_{g2}$  is detected, the output of comparator 3 is logic “true” for Action 5, and else is logic “false” for Action 6. The decision logic in the CPLD can generate the responding driving signal of  $v_{gs2}$ , according to the state machine in Fig. 8(b).

The state machine in Fig. 8(b) enters state 2 from state 1 when the Actions 1 and 4 both are triggered, indicating that CCM is detected. In state 2, the state enters state 3 when Actions 2 and 4 both are triggered. In state 2, the state goes back to state 1 when Actions 2 and 4 both are triggered. It enters state 4 form state 3 when Action 3 happens. However, it also goes back to state 1 form state 3 when Actions 1 and 4 happen due to the CRM being detected. When the state machine arrives at state 4, which means the second resonant peak is detected,  $Q_3$  is turned to absorb the resonance energy of  $L_m$  and  $C_{oss1}$ . During state 4, the state machine keeps

TABLE 2. Key components of prototype circuit.

Symbol	Description	Manufacturer
$Q_1$	IPA65R400CE, 650 V/400 mΩ	Infineon AG
$Q_2$	DMT10H010L, 100 V/ 10 mΩ	Diodes Inc.
$Q_3$	SVF7N65CF, 650 V/1.1 Ω	Silan Microelectronics
$R_{sn}$	20 Ω	
$C_{sn}$	2.2 nF, 100 V, MLCC	Murata
$D_{clamp}$	SS110, 100 V/1 A	Taiwan Semiconductor
SR IC	MP6909	MPS Inc.
flyback IC	RT7740	Richtek Inc.
CPLD	MAX7064S	Altera

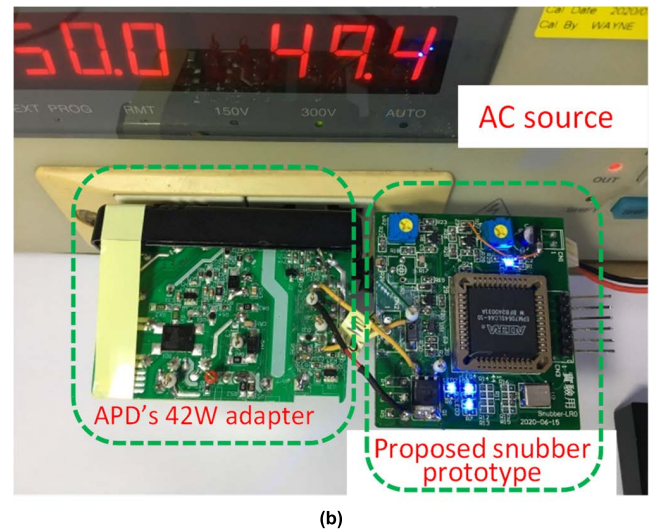
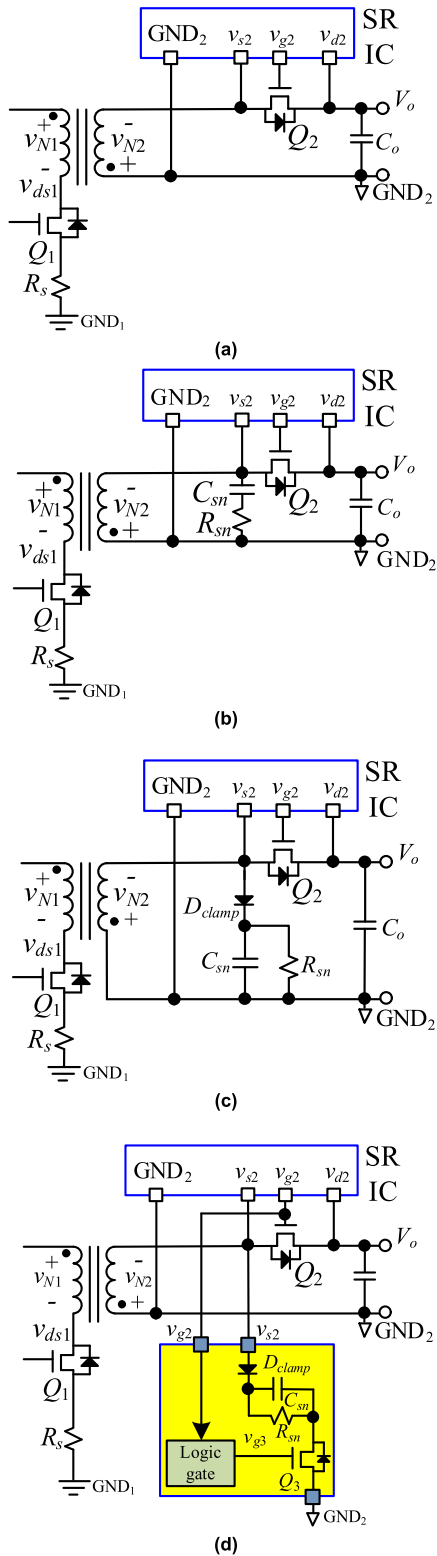


FIGURE 9. Photographs of the original adapter and the proposed prototype: (a) the original adapter and the proposed prototype; (b) bottom side view of the proposed prototype.

detecting  $v_{s2}$ . The state machine moves to state 1 when the condition of Action 4 is satisfied.





**FIGURE 10.** Four circuits for performance comparison: (a) Case 1; (b) Case 2; (c) Case 3; (d) Case 4.

### III. SPECIFICATIONS AND PARAMETERS OF PROTOTYPE

The main component list of this prototype circuit for verification is shown in Table 2.

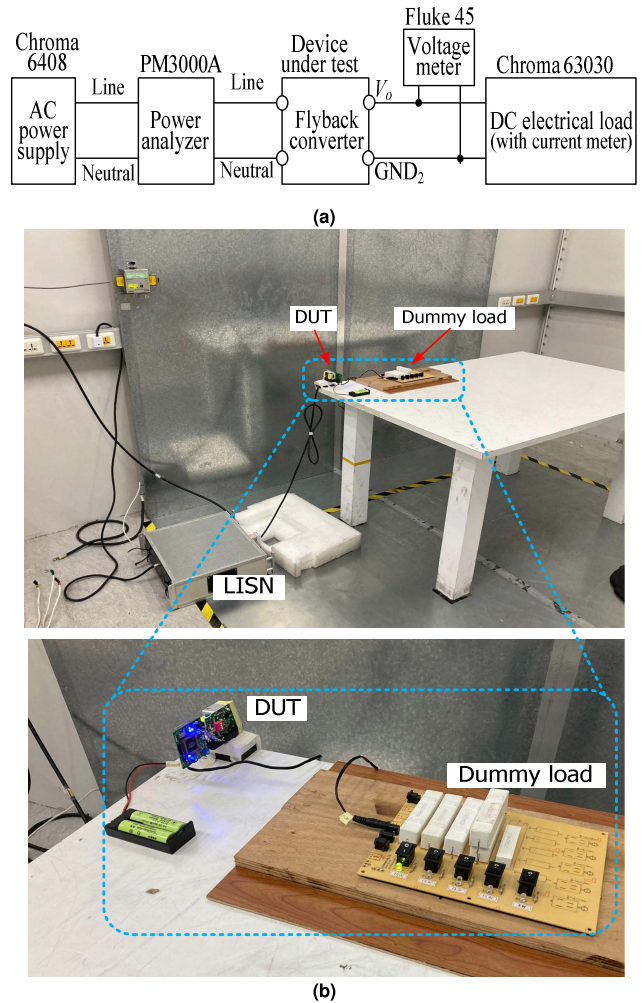


**FIGURE 11.** Test environment: (a) measurement setup of conversion efficiency; (b) measurement setup of conduction EMI.

To shorten the verification time of the new concept, this prototype is built based on the commercial product of a 42 W wall mount adapter by Asian Power Device company as a verification platform as shown in Fig. 9(a).  $V_{in}$  of the prototype is 115 Vac/60 Hz or 230 Vac/50 Hz. Its output voltage and rated output current are 12 V and 3.5 A, respectively. As shown in Fig. 9(b), the prototype board of the proposed snubber is externally added to the original adapter board with an auxiliary powered by a battery to avoid noise pollution from a grid-powered DC power supply when EMI measurement.

There are four test conditions for the prototype, which are applied to the same one adapter platform. the test conditions are as follows:

1) **Case 1:** As shown in Fig. 10(a), the first test condition is the original flyback converter without the secondary-side snubber.

2) **Case 2:** The second test condition is to add the RC snubber to the flyback converter as shown in Fig. 10(b).

3) **Case 3:** As shown in Fig. 10(c), the third test condition is to add the RCD snubber to the flyback converter.

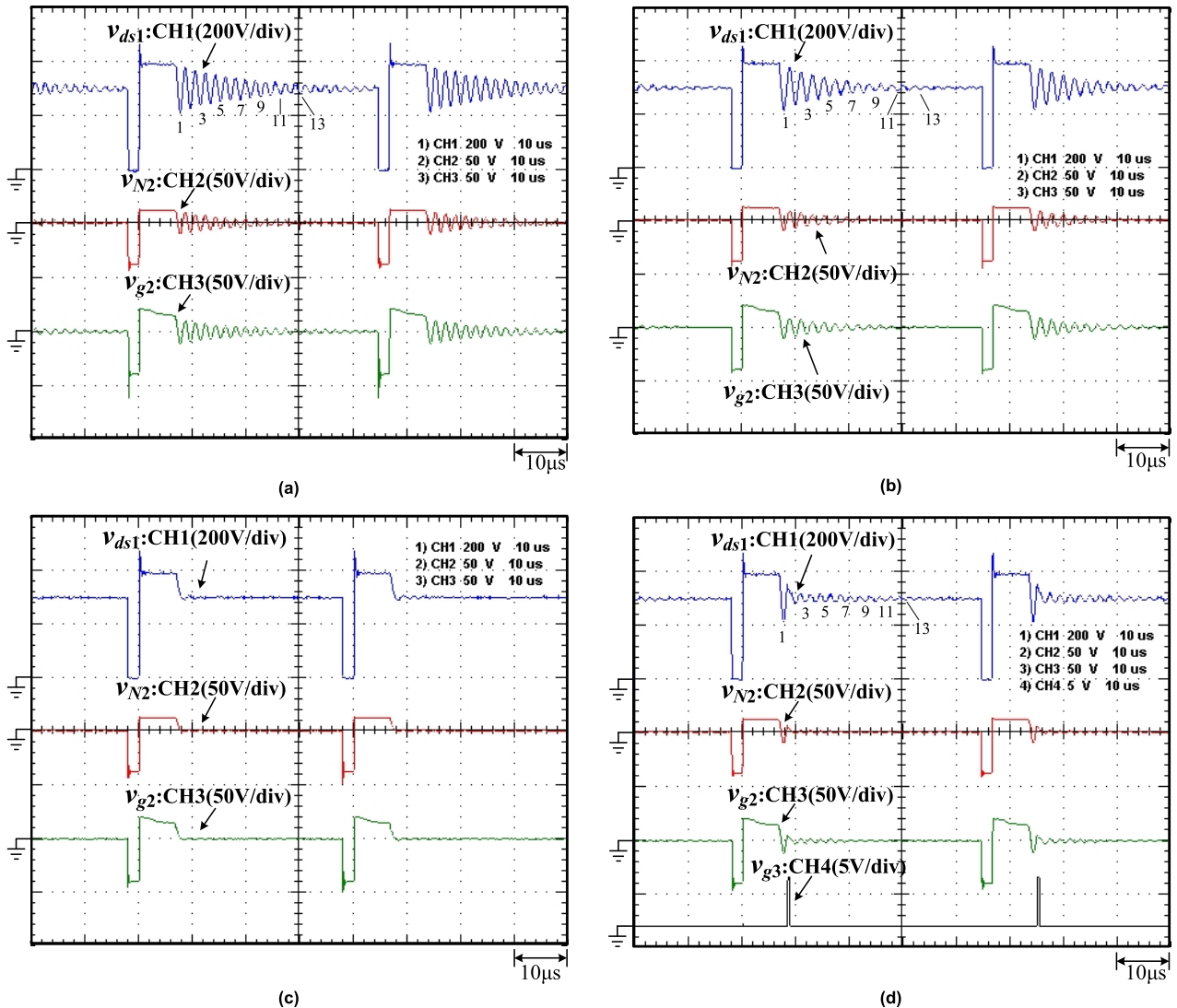


FIGURE 12. Waveforms of  $v_{ds1}$ ,  $v_{N2}$ ,  $v_{G2}$ , and  $v_{G3}$  at 15% load. (a) Case 1; (b) Case 2; (c) Case 3; (d) Case 4.

4) **Case 4:** The fourth test condition is the proposed method as shown in Fig. 10(d).

The measurement setup of the conversion efficiency is shown in Fig. 11(a). As shown in Fig. 11(b), the conduction EMI emissions of the prototype are tested in a qualified EMC certification lab with the measurement setup of the standard CISPR 16-1-2. Because the DUT is a wall-mount type converter with a plastic enclosure, the DUT and its dummy load are located on the table without metal enclosure or bottom plate to simulate the real application.

It should be noted that the proposed circuit and comparative circuits presented in this paper are based on an existing industrial product modified, so the measurements of conversion efficiency and EMI emissions include the original EMI filter stage, the original EMI solutions, and a 1.2 meters output cable with a connector. They contribute to efficiency loss. In addition, to confirm the fairness of the experiment,

the snubbers used in Cases 1 to 4 are built on the same flyback converter as shown in Fig. 9(b). Since the original flyback platform is already an industrial product that has passed EMI regulations of CISPR 22/32 class B, it originally has a sufficient margin of EMI emissions. Therefore, only the differences between different snubbers are discussed in this paper, and not the original design of the platform.

Since the flyback converter operating in CRM and CCM modes does not cause resonance of  $L_m$  and  $C_{oss1}$ , the proposed snubber will be disabled without any effect. So, only the conditions of 15% and 30% of rated load at input voltage 230 Vac are measured and discussed. Due to the internal frequency jittering function of the commercial flyback IC in VSM, the number of DCM valleys is not a fixed value. Under 15% and 30% of the rated load at input voltage 230 Vac, the observed number of DCM resonance valleys are 20 and 10 to 13, respectively.

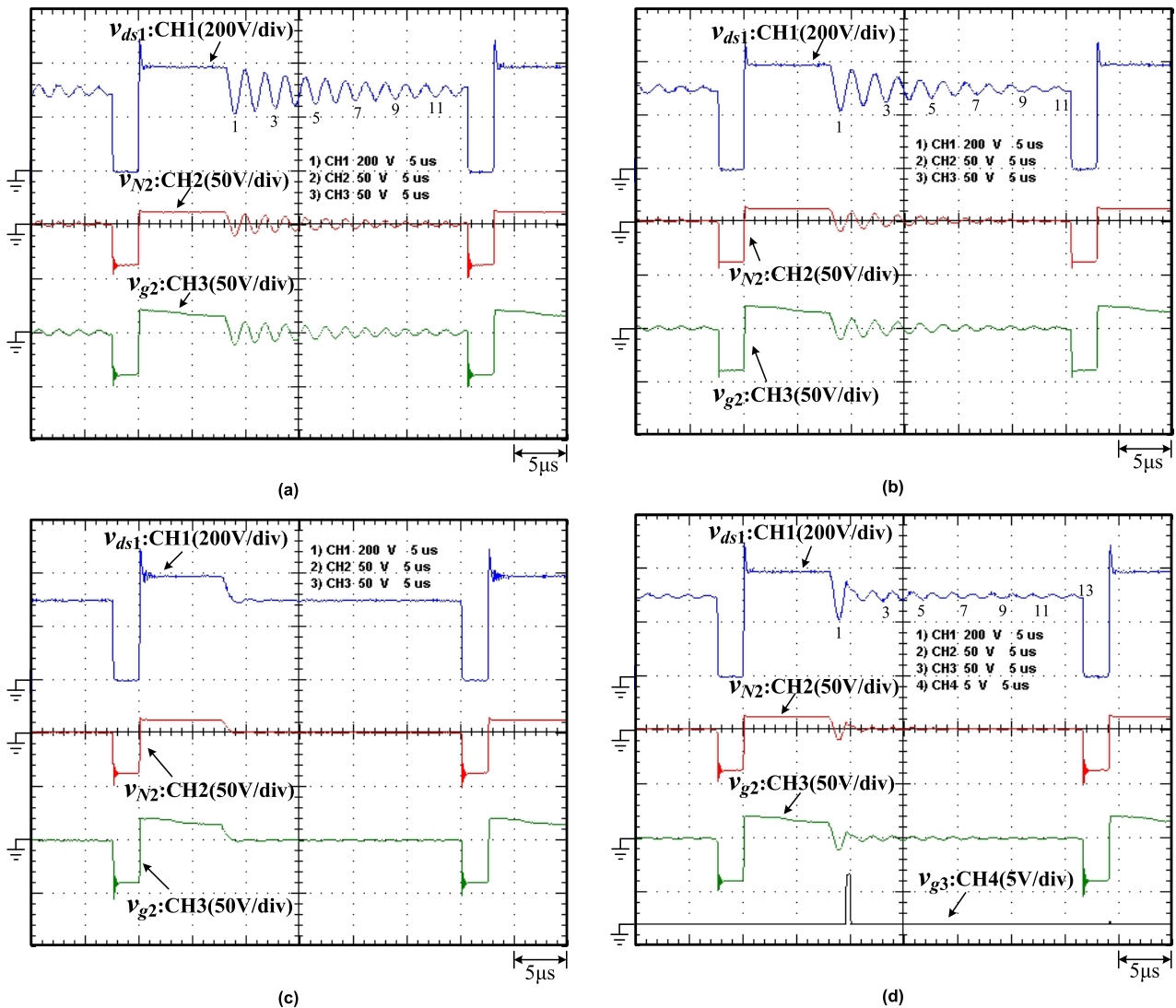


FIGURE 13. Waveforms of  $v_{ds1}$ ,  $v_{N2}$ ,  $v_{g2}$ , and  $v_{g3}$  at 30% load. (a) Case 1; (b) Case 2; (c) Case 3; (d) Case 4.

IV. EXPERIMENTAL WAVEFORMS AND EFFICIENCY

Figs. 12 and 13 show the experimental waveforms of  $v_{ds1}$ ,  $v_{N2}$ , and  $v_{g2}$  from Cases 1 to 4 at 15% load and 30% load, respectively. From Fig. 12, it can be observed that the valley voltage of resonant  $v_{ds1}$  gradually increases along with more numbers of  $v_{ds1}$  resonant cycles. As shown in Figs. 12(a) and 13(a), the energy of the resonant tank in Case 1 is dissipated naturally by parasitic resistance after 13 resonant cycles, even without no additional snubber. In Case 2, as shown in Figs. 12(b) and 13(b), the flyback operates in DCM and decays resonant  $v_{ds1}$  to a negligible value after 10 resonant cycles. Figs. 12(c) and 13(c) show the measured results of Case 3, the resonant waveforms of  $v_{ds1}$ ,  $v_{N2}$ , and  $v_{g2}$  decay completely without significant resonant cycles.

Figs. 12(d) and 13(d) show the waveforms of  $v_{ds1}$ ,  $v_{N2}$ ,  $v_{g2}$ , and  $v_{g3}$  of the proposed Case 4 at 15% load and 30% load,

respectively. The digital controller detects  $v_{g2}$  to generate the  $v_{g3}$  after the first resonant peak of  $v_{ds1}$  is detected. Since the dissipator of Case 4 absorbs energy, the decay time of resonance energy is less than two cycles.

The result of Case 1 means that the resonant energy can still be dissipated by internal parasitic resistance after a long time  $T_{off}$  even if there is no additional snubber. Therefore, more valley numbers do not increase the switching loss of  $C_{oss1}$ . That is, the proposed method does not significantly cause more power loss with forced energy dissipation of the resonance tank after the second resonant valley. When the converter operates under CCM and CRM, the valley number of resonant cycles of  $v_{ds1}$  will be 0 and 1, respectively. The flyback IC needs to detect the first valley of resonance to determine the turned-on time of  $Q_1$  for the next switching period. Therefore, the dissipator is enabled after the first valley to avoid malfunction of flyback controller IC.

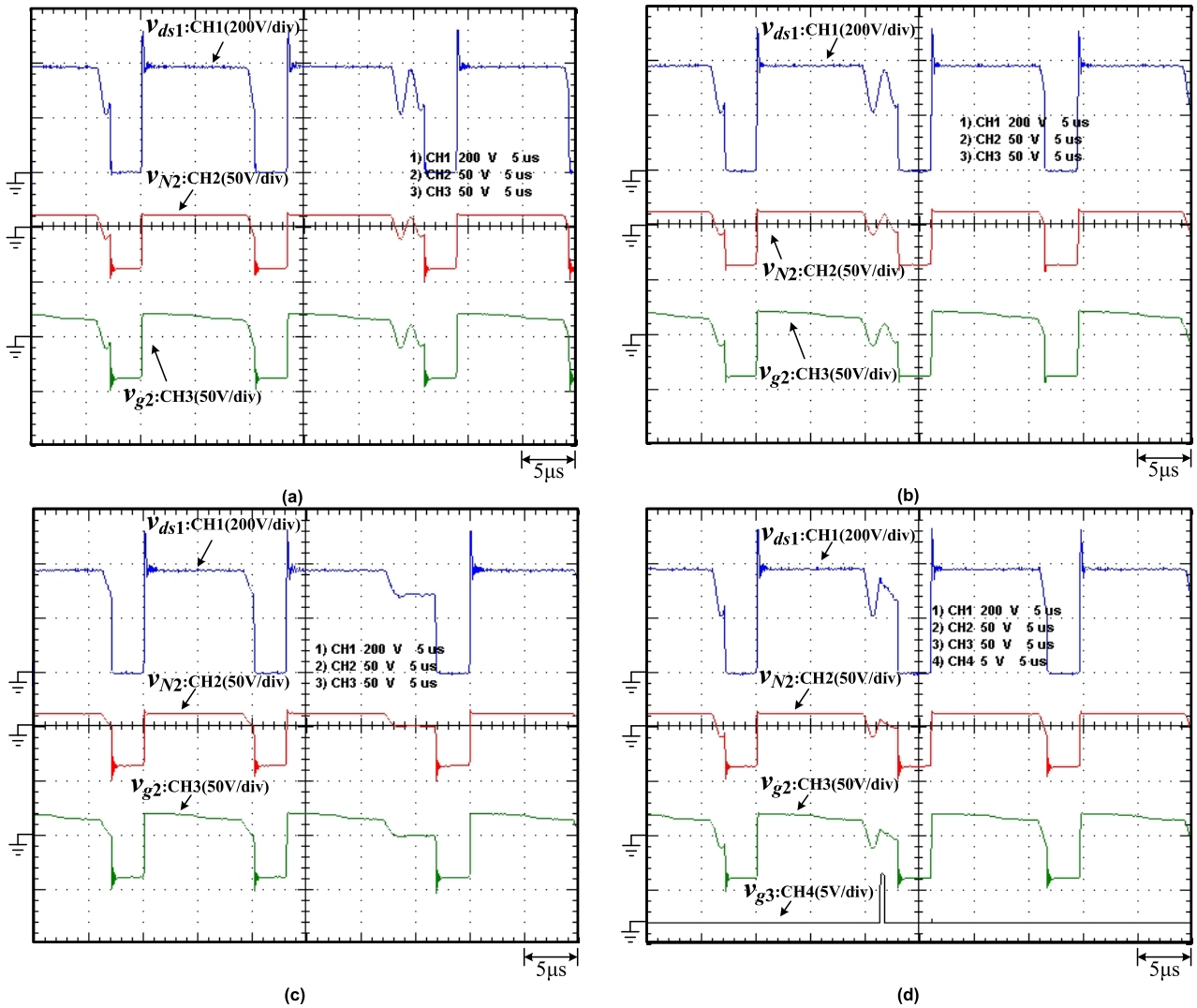


FIGURE 14. Waveforms of  $v_{ds1}$ ,  $v_{N2}$ ,  $v_{gs2}$ , and  $v_{gs3}$  at full load: (a) Case 1; (b) Case 2; (c) Case 3; (d) Case 4.

Fig. 14 shows the experimental waveforms of Cases 1 to 4 under full load. It is seen that the most switching cycles are under CCM or CRM. However, there are still a few DCM cycles, which result from the frequency jitter by the flyback controller IC. Modern commercial flyback ICs have a frequency jitter function to spread the EMI spectrum energy, so the EMI emissions can be reduced further.

Fig. 15 shows the waveforms of  $v_{N2}$ ,  $v_{ds3}$ ,  $v_{gs3}$ , and  $i_{ds3}$  of Case 4 at an input voltage of 115 Vac under 15%, 30%, 60%, 85%, and full load. Fig. 16 shows the waveforms of  $v_{N2}$ ,  $v_{ds3}$ ,  $v_{gs3}$ , and  $i_{ds3}$  of Case 4 at an input voltage of 230 Vac under 15%, 30%, 60%, 85%, and full load.

In Figs. 15 and 16, the number of ring cycles also decreases when the load increases from light load. The switching frequency also increases along with the increased load. Figs. 15(d) and 15(e) show the CCM operation and CRM operation under full load and load of 85%, respectively. The

proposed circuit is disabled when CCM cycle and CRM cycle.

In Figs. 15 and 16, it is observed that the maximum current of  $i_{ds3}$  and peak voltage of  $v_{ds3}$  are under 60 mA and 20 V, respectively. The required voltage rating and current of  $Q_3$  is low to meet a cost-efficient design. It is also observed that a short current glitch occurs when  $Q_3$  remains off-state. This is because when  $v_2$  changes from negative voltage to positive voltage,  $v_{N2}$  charges  $C_{oss3}$  to result in charging current on  $i_{ds3}$ .

As shown in Figs. 15(d), 15(e), and 16(e), since the CCM operation and CRM operation are at heavy load, the  $Q_3$  and the proposed snubber are disabled. But,  $v_{ds3}$  still varies because the  $D_{clamp}$  is reverse biased to make  $v_{ds3}$  float.

Figs. 17(a) and 17(b) is a comparison of the conversion efficiency of Cases 1 to 4 at input voltages of 115 Vac and 230 Vac. It can be observed that Case 1 has the highest conversion efficiency. However, the efficiency result of Case 4 is close to the result of Case 1 as shown in Fig. 17(c).



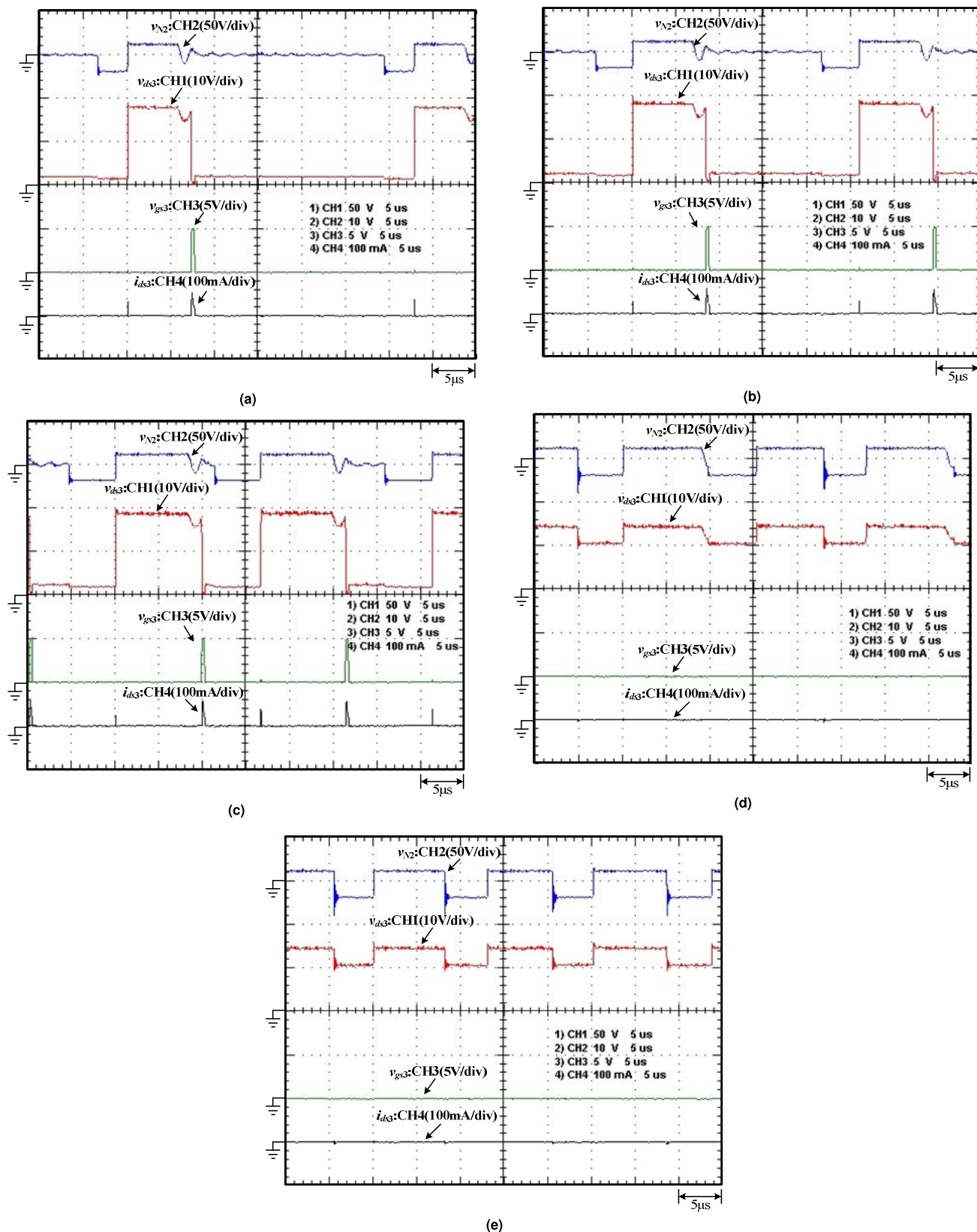


FIGURE 15. Waveforms of  $v_{N2}$ ,  $v_{ds3}$ ,  $v_{gs3}$ , and  $i_{ds3}$  of Case 4 at 115 Vac: (a) 15% load; (b) 30% load; (c) 60% load; (d) 85% load; (e) full load.

Compared to Case 1, the efficiencies of Case 2 at full load under input voltages of 115 Vac and 230 Vac are

decreased by 0.34% and 0.51%, respectively. At 30% load, the conversion efficiencies under input voltages of 115 Vac

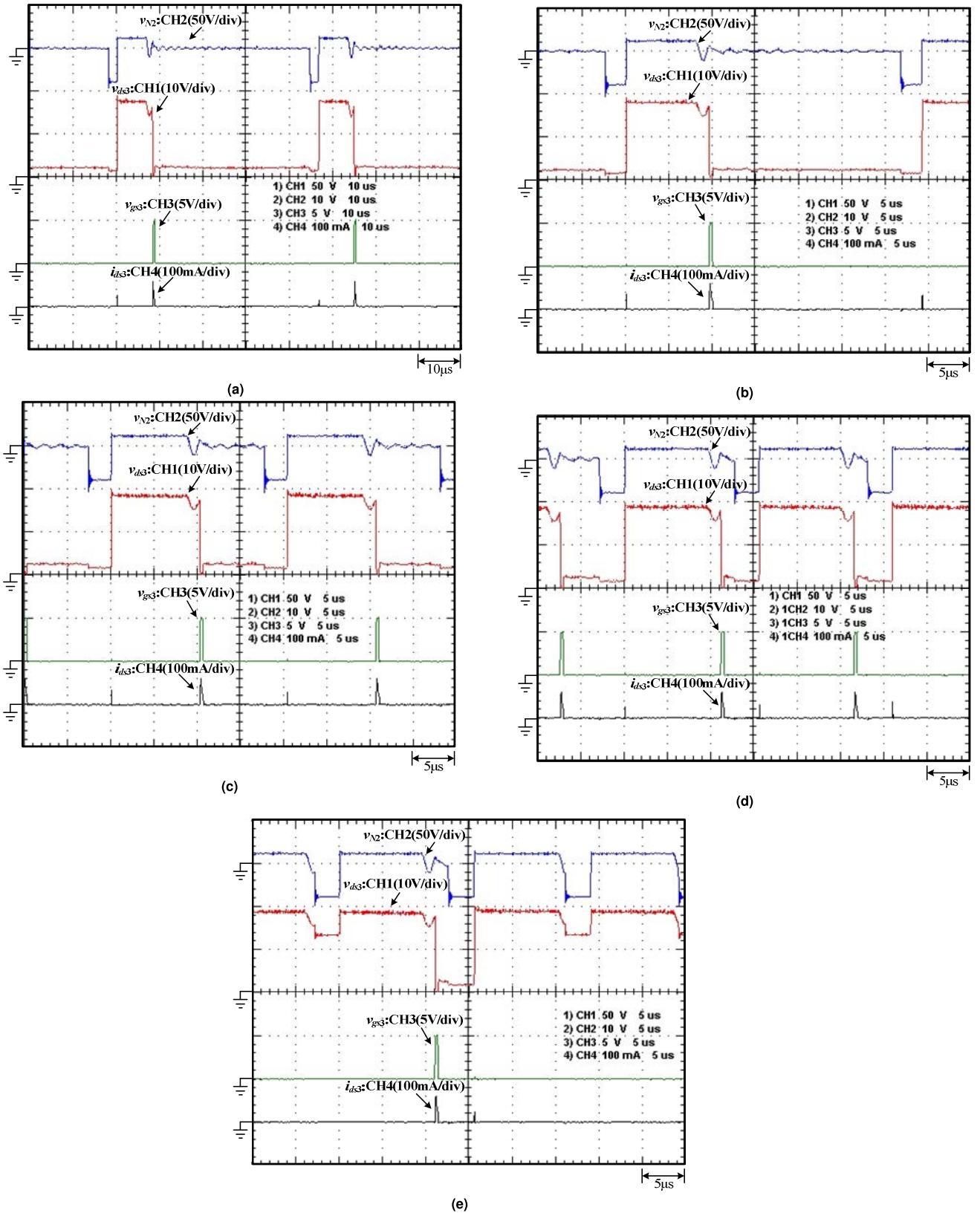
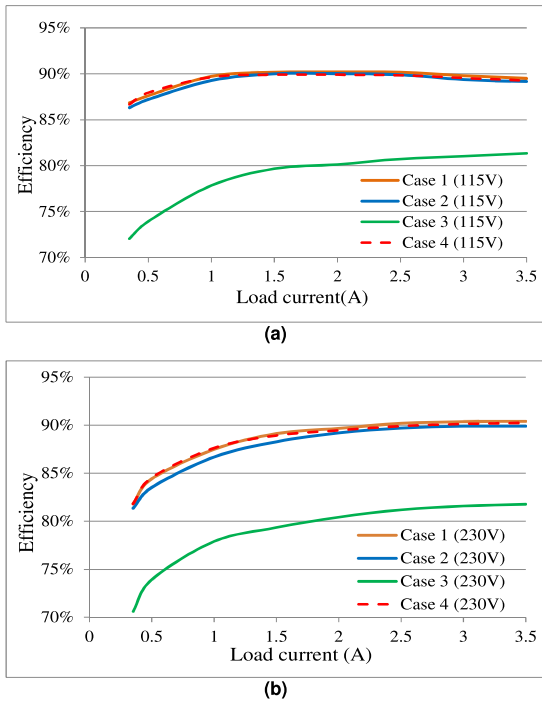


FIGURE 16. Waveforms of  $v_{N2}$ ,  $v_{ds3}$ ,  $v_{gs3}$ , and  $i_{ds3}$  of Case 4 at 230 Vac: (a) 15% load; (b) 30% load; (c) 60% load; (d) 85% load; (e) full load.

and 230 Vac can be decreased by 0.45% and 0.8%, respectively. At 15% load, the efficiency under input voltages of

115 Vac and 230 Vac can be decreased by 0.53% and 0.45%, respectively.



**FIGURE 17. Comparison of measured efficiency of different snubbers under  $V_{in}$  of: (a) 115 Vac/60 Hz; (b) 230 Vac/50 Hz.**

The conversion efficiency of Case 3 significantly decays. The full-load efficiency is reduced by 8%, and the light-load efficiency at 10% load is reduced by 11%, which means that Case 3 is not applicable.

As shown in Fig. 12(a), it can be observed that the resonant frequency of  $L_m$  and  $C_{oss1}$  of Case 1 (without snubber) in DCM is around 450 kHz to 550 kHz. This is the main objective of the proposed method to improve, so the measurement results of the conducted EMI emissions in this frequency range can be observed for comparison. The results of the proposed method of Case 4 are shown in Figs. 12(d) and 13(d). The snubber structure is alike to that of Case 3, but the dissipator is controlled by  $Q_3$ .

**V. PERFORMANCE OF CONDUCTION EMI**

For convenience to show the conduction EMI performance, the measurement results are marked as the limitation margin of Class B conducted emission of CISPR22/32 [25] instead of absolute values. Figs. 18, 19, and 20 show the experimental results of the conducted EMI under 15%, 30%, and full load, respectively. Due to the limitation of EMI equipment, the measured conduction EMI curves can only be shown as peak value curves instead of QP curves and average curves. Fig. 20 shows the measure results of conduction EMI emissions at full load. The performance of these four cases is similar at full load.

Fig. 21 is the comparison chart of conduction EMI emissions at 15%, 30%, and full load. In Fig. 21, a higher margin value means lower EMI emissions and better EMI performance. When under 15% load, the Case 3 has better

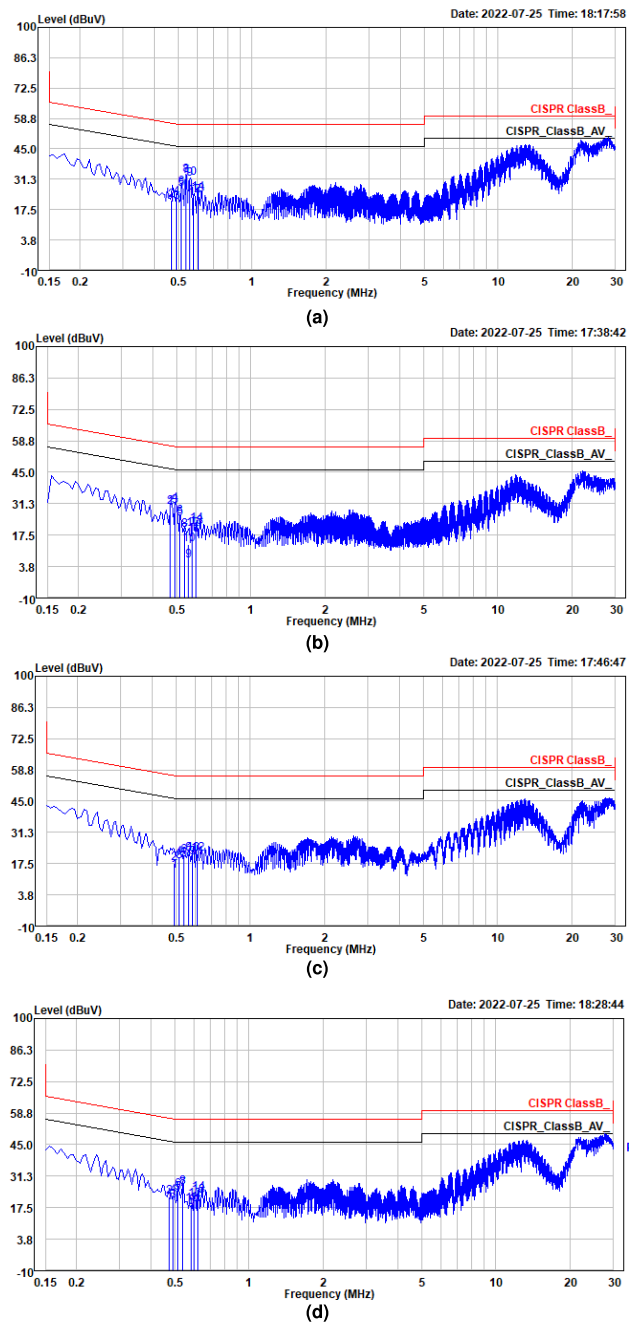


**FIGURE 18. Conduction EMI results at 15% load: (a) Case 1; (b) Case 2; (c) Case 3; (d) Case 4.**

EMI performance but lower power efficiency. The proposed Case 4 provides higher efficiency and better EMI results compared to Cases 2 and 3.

When under 30% load, the proposed Case 4 provides better EMI results compared to Cases 1 and 2. Case 4 has much better power efficiency than the results of Case 3.

The oscillation of  $L_m$  and  $C_{oss1}$  does not occur in CCM and CRM at full load of Cases 1 to 4. EMI emissions in the frequency range of the oscillations of  $L_m$  and  $C_{oss1}$  are expected to be the same result as shown in Fig. 21. From the

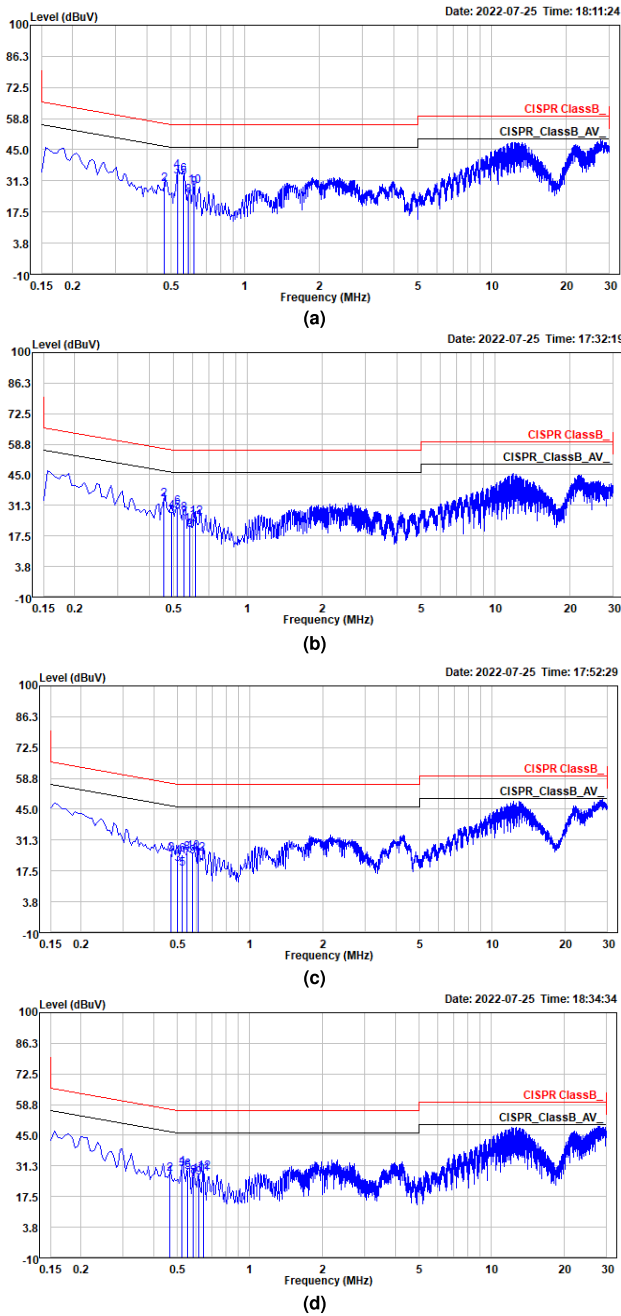


FIGURE 19. Conduction EMI results at 30% load: (a) Case 1; (b) Case 2; (c) Case 3; (d) Case 4.

experimental results of Case 4, it can be observed that the conduction EMI emissions are reduced in QP and average to verify that the proposed method has a significant EMI suppression effect.

Table 3 shows the comparison of theoretical power dissipation of Cases 1 to 4 in their snubber. It is seen that the loss calculation formula of the proposed method is the same as the formula of Case 1. This can explain why they have similar experimental results of conversion efficiency.

In this study, the CPLD chip is used as a verification of the proposed concept, and in the future, the proposed snubber

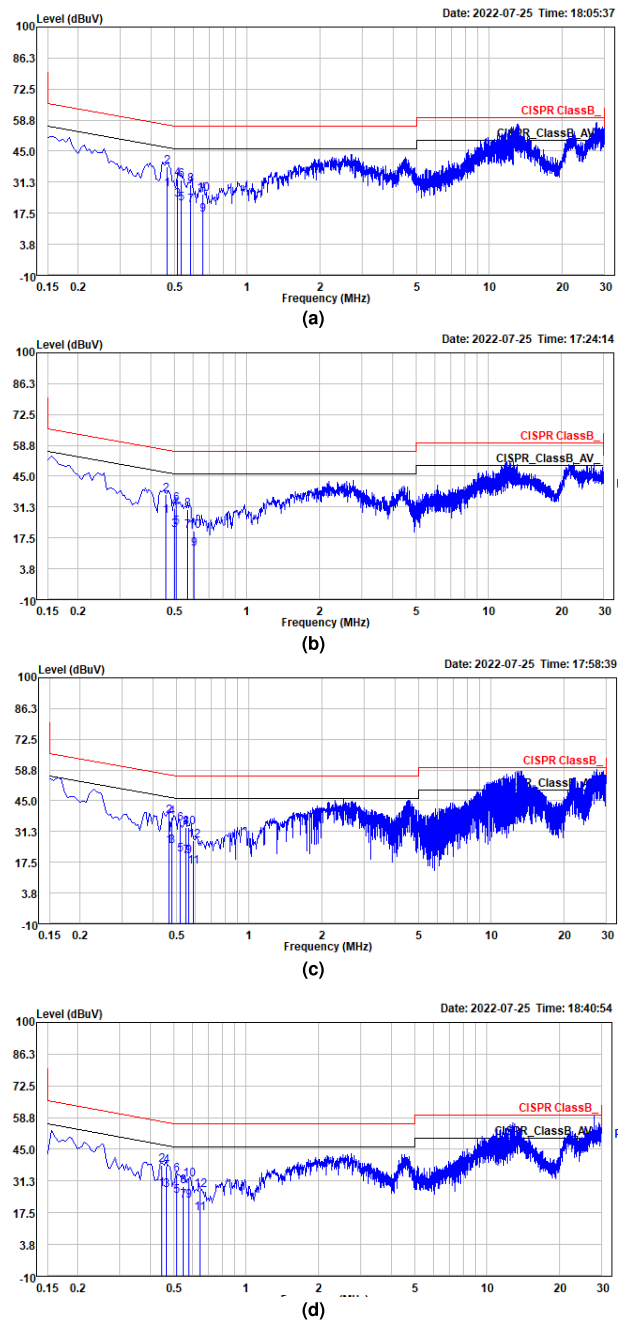


FIGURE 20. Conduction EMI results at full load: (a) Case 1; (b) Case 2; (c) Case 3; (d) Case 4.

could be integrated into a single chip of SR controller by chip design.  $Q_3$  and  $R_{sn}$  can be built into the SR IC, and  $C_{sn}$  can be integrated into the SR IC by silicon wafer-based integrated capacitors [26], [27]. The block diagram of the concept circuit is shown in Fig. 22.

By integrating the proposed snubber with the SR IC, the snubber can be based on programmable digital parameters, so that no external components are required. That also takes no more space on the printed circuit board. Furthermore, the parameters of the proposed snubbers can be online changed



TABLE 3. Comparison of all cases.

Snubber solution	Case 1			Case 2			Case 3			Case 4		
Type of snubber	No snubber			(R+C) Snubber			(R//C)+D snubber			Proposed snubber		
Resonance cycle	>10			5~10			0~1			1~2		
Estimation of power dissipation from snubber	$\frac{f_{sw} \cdot C_{oss1} \left( \left( V_{in} + V_o \cdot \frac{N_1}{N_2} \right)^2 - V_{in}^2 \right)}{2}$			$\frac{f_{sw} \cdot C_{oss1} \left( \left( V_{in} + V_o \cdot \frac{N_1}{N_2} \right)^2 - V_{in}^2 \right)}{2}$ $+\frac{f_{sw} \cdot C_{sn} \left( V_{in} \cdot \frac{N_1}{N_2} + V_o \right)^2}{2}$			$\frac{f_{sw} \cdot C_{oss1} \left( \left( V_{in} + V_o \cdot \frac{N_1}{N_2} \right)^2 - V_{in}^2 \right)}{2}$ $+\frac{C_{sn} \left( V_{in} \cdot \frac{N_1}{N_2} + V_o \right)^2}{2} + T_{oss(Q2)} \cdot \frac{V_o^2}{R_{sn}}$			$\frac{f_{sw} \cdot C_{oss1} \left( \left( V_{in} + V_o \cdot \frac{N_1}{N_2} \right)^2 - V_{in}^2 \right)}{2}$		
Percentage of rated load	15%	30%	100%	15%	30%	100%	15%	30%	100%	15%	30%	100%
Resonant Frequency $f_r$ (kHz)	539	532	516	494	458	511	539	548	518	537	525	515
Quasi peak (dBμV) (margin)	22.9	20.6	23.3	25.3	23	23.5	35	22.8	21.3	27	25.3	22.1
Average (dBμV) (margin)	13.3	12.7	22.3	15.9	14.7	23.7	26.8	30.4	25	20.5	16.4	21.2
Efficiency (%) (115 Vac input)	87.62	89.72	89.5	87.20	89.27	89.16	73.94	77.84	81.35	87.74	89.64	89.27
Efficiency (%) (230 Vac input)	84.43	87.49	90.41	83.53	86.69	89.9	73.93	77.91	81.78	84.54	87.63	90.25

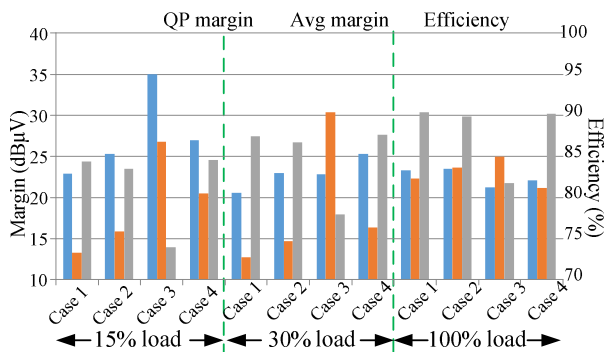


FIGURE 21. Comparison of quasi-peak margin and average margin at 15% and 30% of the rated load, respectively.

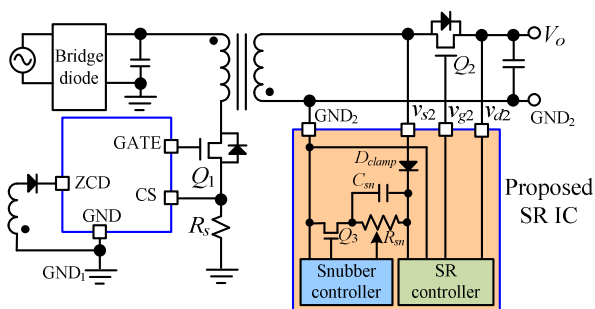


FIGURE 22. Combination of SR IC and the proposed snubber.

according to different operating modes to improve EMI and efficiency under different operation conditions.

### VI. CONCLUSION

Dissipative snubbers are historic circuits. However, they are still popular design solutions for cost-efficient flyback converters. In this paper, the proposed method is to activate the dissipative snubber only when the noise is occurring, then disabled after the noise source is decayed or disappears. Therefore, the snubber selectively absorbs EMI noise.

The flyback converter prototype is used to successfully verify the proposed concept. Compared with the traditional dissipative snubber used in flyback converters, the proposed method effectively eliminates the resonance effect in DCM.

Because the proposed snubber is not connected to the main circuit all the time, it can provide lower EMI emissions and maintain its conversion efficiency. The proposed method is simple, and can be configured and programmed via software. It is also possible to be integrated with synchronous rectifier chips in the future, so that no external components are required.

The proposed snubber is not only applied to flyback converter, but may also be used for other converter topologies.

## REFERENCES

- [1] Datasheet. 'MP6909' Monolithic Power Systems. Accessed: Jun. 6, 2018. [Online]. Available: <https://www.monolithicpower.com/>
- [2] Datasheet. 'RT7740' Richtek Corporation. Accessed: Jul. 2018. [Online]. Available: <https://www.richtek.com/>
- [3] Datasheet. 'LD5523' Leadtrend Corporation. Accessed: Oct. 2016. [Online]. Available: <https://www.leadtrend.com.tw/>
- [4] K.-H. Chen and T.-J. Liang, "Design of quasi-resonant flyback converter control IC with DCM and CCM operation," in *Proc. Int. Power Electron. Conf. (IPEC-Hiroshima-ECCE ASIA)*, Hiroshima, Japan, May 2014, pp. 2750–2753.
- [5] Y. Bai, X. Yang, D. Zhang, L. Li, and W. Chen, "Frequency jitter modulation method for quasi-resonant flyback converter to mitigate EMI," in *Proc. IEEE 8th Int. Power Electron. Motion Control Conf. (IPEMC-ECCE Asia)*, Hefei, China, May 2016, pp. 2161–2167.
- [6] Infineon AG, Application Note. *Quasi-Resonant and Fixed-Frequency Flyback Comparison*. Accessed: Jun. 1, 2018. [Online]. Available: <https://www.infineon.com/>
- [7] G.-B. Koo, S.-C. Moon, and J.-T. Kim, "A new valley-detection method for the quasi-resonance switching," in *Proc. 25th Annu. IEEE Appl. Power Electron. Conf. Expo. (APEC)*, Palm Springs, CA, USA, Feb. 2010, pp. 540–543.
- [8] C. Basso, "The dark side of flyback converters," presented at the IEEE APEC Educ. Seminar, Fort Worth, TX, USA, 2011.
- [9] W. Cheng, X. He, S. Xu, and W. Sun, "Analysis and accurate modeling of a flyback converter on conducted EMI," in *Proc. 9th Int. Conf. Power Electron. ECCE Asia (ICPE-ECCE Asia)*, Seoul, South Korea, Jun. 2015, pp. 2275–2281.
- [10] P. Meng, J. Zhang, H. Chen, Z. Qian, and Y. Shen, "Characterizing noise source and coupling path in flyback converter for common-mode noise prediction," in *Proc. 26th Annu. IEEE Appl. Power Electron. Conf. Expo. (APEC)*, Fort Worth, TX, USA, Mar. 2011, pp. 1704–1709.
- [11] Y.-T. Yau and T.-L. Hung, "Lossless snubber for GaN-based flyback converter with common mode noise consideration," *IEEE Access*, vol. 10, pp. 56652–56667, 2022.
- [12] M. Rucinski, P. Musznicki, and P. J. Chrzan, "Electromagnetic interference frequencies prediction model of flyback converter for snubber design," *IET Power Electron.*, vol. 8, no. 6, pp. 994–999, Jun. 2015.
- [13] A. Hren, J. Korelic, and M. Milanovic, "RC-RCD clamp circuit for ringing losses reduction in a flyback converter," *IEEE Trans. Circuits Syst. II, Exp. Briefs*, vol. 53, no. 5, pp. 369–373, May 2006.
- [14] K. Scott and Z. Qian. *No-Opto Flyback DC/DC Converters & Snubber Protection Circuits*. [Online]. Available: [www.analog.com/en/technical-articles/no-opto-flyback-dc-dc-converters-snubber-protection-circuits.html](http://www.analog.com/en/technical-articles/no-opto-flyback-dc-dc-converters-snubber-protection-circuits.html)
- [15] R. Watson, F. C. Lee, and G. C. Hua, "Utilization of an active-clamp circuit to achieve soft switching in flyback converters," *IEEE Trans. Power Electron.*, vol. 11, no. 1, pp. 162–169, Jan. 1996.
- [16] Y. T. Yau, W. Z. Jiang, and K. I. Hwu, "Light-load efficiency improvement for flyback converter based on hybrid clamp circuit," in *Proc. IEEE Int. Conf. Ind. Technol. (ICIT)*, Taipei, Taiwan, Mar. 2016, pp. 329–333.
- [17] A. Zaman and A. Radic, "How to design and implement an adapter power supply with active clamp flyback: An all silicon design methodology," *IEEE Power Electron. Mag.*, vol. 7, no. 4, pp. 36–43, Dec. 2020.
- [18] C. Vartak, A. Abramovitz, and K. M. Smedley, "Analysis and design of energy regenerative snubber for transformer isolated converters," *IEEE Trans. Power Electron.*, vol. 29, no. 11, pp. 6030–6040, Nov. 2014.
- [19] E. Dzhunusbekov and S. Orzabayev, "A new passive lossless snubber," *IEEE Trans. Power Electron.*, vol. 36, no. 8, pp. 9263–9272, Aug. 2021.
- [20] A. Abramovitz, C.-S. Liao, and K. Smedley, "State-plane analysis of regenerative snubber for flyback converters," *IEEE Trans. Power Electron.*, vol. 28, no. 11, pp. 5323–5332, Nov. 2013.
- [21] M. Mohammadi, E. Adib, and M. R. Yazdani, "Family of soft-switching single-switch PWM converters with lossless passive snubber," *IEEE Trans. Ind. Electron.*, vol. 62, no. 6, pp. 3473–3481, Jun. 2015.
- [22] S. M. Tadvin, S. R. B. Shah, and M. R. T. Hossain, "A brief review of snubber circuits for flyback converter," in *Proc. IEEE I2CT*, Pune, India, Apr. 2018, pp. 1–5.
- [23] C.-S. Liao and K. M. Smedley, "Design of high efficiency flyback converter with energy regenerative snubber," in *Proc. 23rd Annu. IEEE Appl. Power Electron. Conf. Expo.*, Austin, TX, USA, Feb. 2008, pp. 796–800.
- [24] A. Alganidi and G. Moschopoulos, "A comparative study of two passive regenerative snubbers for flyback converters," in *Proc. IEEE Int. Symp. Circuits Syst. (ISCAS)*, Florence, Italy, May 2018, pp. 1–4.
- [25] *Electromagnetic Compatibility of Multimedia Equipment—Emission Requirements*, 2nd ed., CISPR, Geneva, Switzerland, Mar. 2015, vol. 32, p. 2015.
- [26] S. Banzhaf, S. Schwaiger, T. Erlbacher, A. J. Bauer, L. Frey, and L. Frey, "Post-trench processing of silicon deep trench capacitors for power electronic applications," in *Proc. 28th Int. Symp. Power Semiconductor Devices ICs (ISPSD)*, Prague, Czech Republic, Jun. 2016, pp. 399–402.
- [27] S. Jacqueline, C. Bunel, and L. Lengignon, "Outstanding reliability performances of silicon capacitors for 200° C automotive applications," in *Proc. IEEE 70th Electron. Compon. Technol. Conf. (ECTC)*, Orlando, FL, USA, Jun. 2020, pp. 2133–2138.



**YEU-TORNG YAU** (Member, IEEE) received the B.S. and M.S. degrees in electrical engineering from Tamkang University, Tamsui, Taiwan, in 2002 and 2004, respectively, and the Ph.D. degree in electrical engineering from the National Taipei University of Technology, Taipei, Taiwan, in 2012. In 2002, he was with AcBel Company for six months. From 2005 to 2011, he was a Researcher with the Industrial Technology Research Institute, Hsinchu, Taiwan. From 2011 to 2014, he was a Senior Engineer with Leadtrend Technology Corporation and Advanced Analog Technology. From 2014 to 2020, he was an Engineer at Asian Power Devices Inc., Taoyuan, Taiwan. He is currently an Assistant Professor with the National Chin-Yi University of Technology, Taichung, Taiwan. His research interests include power electronics, converter topology, electromagnetic compatibility, and digital control.



**TSUNG-LIANG HUNG** received the B.S. and M.S. degrees in electrical engineering from the National Yunlin University of Science and Technology, Yunlin, Taiwan, in 2000 and 2002, respectively. From 2002 to 2013, he was a Supervisor and the Manager with Ambit, Foxconn, Ampower, and Leadtrend Technology Corporation. He is currently the Manager at the Technology Center, Asian Power Devices Inc. His research interests include power electronics, converter topology, and control behavior.

...